Intrinsic noise and division cycle effects on an abstract biological oscillator

Michail Stamatakis[a] and Nikos V. Mantzaris
Department of Chemical and Biomolecular Engineering, Rice University, Houston, Texas 77005, USA

(Received 16 February 2010; accepted 11 August 2010; published online 24 September 2010)

Oscillatory dynamics are common in biological pathways, emerging from the coupling of positive and negative feedback loops. Due to the small numbers of molecules typically contained in cellular volumes, stochastic effects may play an important role in system behavior. Thus, for moderate noise strengths, stochasticity has been shown to enhance signal-to-noise ratios or even induce oscillations in a class of phenomena referred to as "stochastic resonance" and "coherence resonance," respectively. Furthermore, the biological oscillators are subject to influences from the division cycle of the cell. In this paper we consider a biologically relevant oscillator and investigate the effect of intrinsic noise as well as division cycle which encompasses the processes of growth, DNA duplication, and cell division. We first construct a minimal reaction network which can oscillate in the presence of large or negligible timescale separation. We then derive corresponding deterministic and stochastic models and compare their dynamical behaviors with respect to (i) the extent of the parameter space where each model can exhibit oscillatory behavior and (ii) the oscillation characteristics, namely, the amplitude and the period. We further incorporate division cycle effects on both models and investigate the effect of growth rate on system behavior. Our results show that in the presence but not in the absence of large timescale separation, coherence resonance effects result in extending the oscillatory region and lowering the period for the stochastic model. When the division cycle is taken into account, the oscillatory region of the deterministic model is shown to extend or shrink for moderate or high growth rates, respectively. Further, under the influence of the division cycle, the stochastic model can oscillate for parameter sets for which the deterministic model does not. The division cycle is also found to be able to resonate with the oscillator, thereby enhancing oscillation robustness. The results of this study can give valuable insight into the complex interplay between oscillatory intracellular dynamics and various noise sources, stemming from gene expression, cell growth, and division. © *2010 American Institute of Physics*. [doi:10.1063/1.3484868]

Oscillations in biological systems are influenced by the intrinsic stochasticity in the occurrence of reaction events, as well as the division cycle. Previous work has focused on the effect of noise strength on the signal-to-noise ratio of the oscillation. Stochastic resonance effects have thus been revealed: for moderate noise strengths the signal-to-noise ratio is maximized. In this paper we present a comprehensive modeling study of a biologically relevant oscillatory reaction network to isolate the effects of timescale separation, intrinsic noise, and division cycle. To this end, we compare corresponding deterministic and stochastic models at different parameter regions, where timescale separation is present or absent. To isolate the effect of division cycle we compare models that account for the processes of growth, DNA production, and division, with models that neglect these processes. We find that in the presence, but not in the absence of timescale separation, intrinsic noise extends the region of the parameter space where oscillations are observed and lowers the period. Cell growth and DNA production can enlarge or shrink the oscillatory region for moderate or higher growth rates, respectively. In the presence of stochasticity in DNA duplication and division, the division cycle can introduce robust oscillations in regions where the deterministic model does not oscillate. The conclusions drawn from our comparisons can provide significant insight into the complex interplay between oscillatory dynamics and the various sources of noise that exist in the cell.

I. INTRODUCTION

Oscillatory dynamics are ubiquitous in biological systems, with typical examples being the circadian rhythms,[1] Ca^{2+} dynamics,[2] and the cell cycle.[3,4] In these systems, there typically exist coupled positive and negative feedbacks which generate the oscillatory behavior. For example, the core oscillator responsible for circadian rhythms in the fungus *Neurospora crassa* operates as follows:[5] two transcription factors, namely, the white collar proteins WC-1 and WC-2, assemble into a complex (WCC) and induce production of the frequency (FRQ) protein (positive feedback). FRQ enters the nucleus and represses the accumulation of *frq* mRNA through, what is believed to be, a negative feedback loop to WCC. Subsequently, FRQ is accumulated again and the process repeats itself. Core circadian oscillator modules

[a]Author to whom correspondence should be addressed. Present address: University of Delaware-Chemical Engineering, 150 Academy Street, Newark, DE 19716, USA. Telephone: +1-302-831-8705. Electronic mail: mstam@alumni.rice.edu.

that exist in other organisms share the common characteristic of interacting positive and negative feedback loops.[6]

In the case of the calcium system of mammalian cells,[2] intracellular Ca^{2+} is stored into the endoplasmic reticulum (ER) or the sarcoplasmid reticulum and is secreted by channels sensitive to IP_3 or ryanodine. Ca^{2+} is able to interact with these receptors, thereby inducing its own secretion through a positive feedback [calcium-induced calcium release (CICR)]. Once the Ca^{2+} concentration into the cytosol becomes high enough, ATPase pumps that exist in the surface of the ER return Ca^{2+} back into the ER; this interaction can be thought as a negative feedback. After the Ca^{2+} concentration is restored to basal levels, the ER channels open again releasing Ca^{2+} into the cytoplasm and the process repeats itself. Other mechanisms (Ca^{2+} fluxes from and to the extracellular space or the mitochondria, buffering activity of proteins) can modulate the calcium oscillations. However, it is essentially the existence of coupled positive (CICR) and negative (ATPase pump) feedback loops that generates oscillations in the intracellular Ca^{2+} concentration.

Finally, in the case of a mitotic oscillator, cyclin B and CDK1 dimerize forming the M-phase promoting factor (MPF). Once MPF is activated by the cyclin dependent kinase CDK1, it subsequently activates the anaphase promoting complex (APC) through a positive feedback. APC in turn degrades cyclin B, thereby inactivating MPF;[4] this interaction generates the negative feedback. If multiple positive and negative feedbacks exist, their coupling can lead to complex oscillatory responses such as birythmicity and chaos.[7]

The oscillatory dynamics encountered in cellular systems are subject to an extra source of complexity: due to the small volumes and numbers of molecules participating in the biochemical events, the stochasticity in the occurrence of the latter is significant.[8,9] This source of stochasticity, termed intrinsic noise,[10] may introduce fluctuations in the periods and the amplitudes of biological oscillators, and thus, it has been proposed that noise resistance mechanisms must be considered in models of such systems.[11]

The interplay between intrinsic noise and oscillatory behavior is not always detrimental though. It can also give rise to phenomena referred to as "stochastic resonance."[12] This term initially referred to the entrainment of noise-induced transitions by a periodic signal,[13] but it has since been generalized to refer to cooperative effects between stochasticity and periodicity that lead to an increase of signal-to-noise ratio for moderate levels of noise. Stochastic resonance has been shown to promote the accuracy of biological oscillators such as circadian clocks,[14] and artificial genetic oscillators,[15,16] and has also been characterized in excitable systems.[17] Since the strength of the stochastic resonance depends on the magnitude of the noise, tuning the latter can facilitate the detection of weak signals and improve information processing in biology.[18,19]

On the other hand, noise has been shown to induce oscillatory behavior in systems for which deterministic models do not oscillate but exhibit excitability. This effect termed "coherence resonance"[20] has been observed in models of circadian clocks[21,22] and Ca^{2+} dynamics,[23,24] the cell cycle,[25] as well as theoretical models of excitability.[17] In these systems, an excitable steady state gets continuously perturbed by noise, thereby giving rise to a train of repetitive spikes. For example, for the Ca^{2+} system, models that incorporate stochasticity in the binding and unbinding events of Ca^{2+} and IP_3 to the corresponding sites have been shown to reproduce oscillation-like behavior, whereas deterministic models do not.[26]

Noise in biological systems though does not stem solely from stochasticity in intracellular reactions. Apart from the intrinsic noise sources, extrinsic noise contributions also influence the behavior of these systems.[10] In particular, during the course of a division cycle, the volume of the cell doubles, along with the molecular contents of DNA, and the metabolic and regulatory machinery of the cell (DNA and RNA polymerases, activators and repressors, etc.). The molecular contents of these species are also subject to stochastic fluctuations and finally, upon partitioning, the two daughters may inherit different number of molecules, further contributing to the extrinsic noise. Extrinsic noise effects have been investigated for a variety of genetic architectures.[10,27–30] Yet, the effects of extrinsic noise on oscillatory dynamics remain unclear. More specifically, the effects of DNA accumulation right after a DNA duplication event, and the dilution due to cell volume expansion during growth, have not been investigated.

In this paper we use a comparative approach to elucidate the effect of timescale separation, as well as intrinsic and extrinsic noise sources on a biologically relevant oscillatory reaction network. To do so, we first construct an abstract, minimal oscillator involving two species, an activator and an inhibitor, and incorporating a single positive and a single negative feedback loop. We subsequently derive a deterministic model using mass action kinetics and analyze its asymptotic and transient behavior. The model is found to be able to exhibit threshold behavior depending on the value of a parameter controlling the timescale separation between the activator and inhibitor dynamics. We then incorporate growth and DNA production using a continuum model formulation[31] and study the effect of deterministic division cycle dynamics.

Using the same reaction network, we subsequently derive the corresponding stochastic model and employ Gillespie's algorithm to simulate the stochastic dynamics[32] at various regions of the parameter space. We further incorporate cell growth, DNA duplication, and division on the stochastic model and simulate the resulting master equation. In the latter, DNA duplication is treated as a discrete event that occurs randomly in time and results in the production of new operator molecules, which, upon division, are partitioned to the new daughters using hypergeometric random deviates. Thus, we isolate the effects of stochasticity on system behavior by comparing the predictions of the stochastic and deterministic models; we demonstrate the effect of timescale separation by comparing the cases where the system does or does not exhibit large separation; and we finally elucidate the effect of extrinsic noise stemming from the division cycle by comparing the models that take into account growth, DNA production, and division with those that do not.

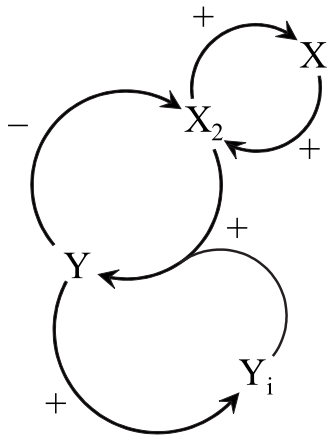

FIG. 1. Interaction diagram for the key species of the biological oscillator network (X: activator monomer, X_2: activator dimer, Y_i: inactive degrader, Y: active degrader, + and − denote positive and negative feedbacks, respectively).

II. REACTION NETWORK

The molecular mechanisms included in our reaction network appear schematically in Fig. 1. The key species are the activator X, whose dimer X_2 exerts the positive feedback, and the degrader Y, which exists in the inactive (Y_i) and the active (Y) states.

The constitutive expression of the activator monomer X from an operator site is modeled as a first order reaction,

$$O \xrightarrow{k_0} O + X. \tag{1}$$

The dimerization of the activator is assumed to be a reversible reaction with dissociation constant denoted by β,

$$2X \xrightarrow{\chi} X_2, \tag{2}$$

$$X_2 \xrightarrow{\beta\chi} 2X. \tag{3}$$

Once dimerized, the activator can exert the positive feedback: the dimer X_2 binds reversibly to the operator site, with a dissociation constant denoted by α,

$$O + X_2 \xrightarrow{\phi} OX_2, \tag{4}$$

$$OX_2 \xrightarrow{\alpha\phi} O + X_2. \tag{5}$$

The bound operator also expresses the protein X,

$$OX_2 \xrightarrow{k_1} OX_2 + X. \tag{6}$$

We note that the kinetic constant for the expression of X from reaction (6) is assumed to be higher than that of the constitutive expression, $(k_1 > k_0)$. Thus, this binding enhances the production of the activator monomer X compared to the constitutive expression from a free operator site [reaction (1)].

Furthermore, the dimer X_2 activates species Y in a reaction that follows second order kinetics. This action provides the coupling between positive and negative feedbacks,

TABLE I. Symbols used for the species.

Symbol	Species denoted
O	Operator
X	Activator monomer
X_2	Activator dimer
OX_2	Activator dimer-operator complex
Y_i	Inactive degrader
Y	Activated degrader
∅	Generic source or sink

$$Y_i + X_2 \xrightarrow{k_2} Y + X_2. \tag{7}$$

Once activated, Y can exert its negative feedback, as it specifically degrades X and its dimer X_2 according to the following reactions:

$$X + Y \xrightarrow{\lambda_1} Y, \tag{8}$$

$$X_2 + Y \xrightarrow{\lambda_2} Y. \tag{9}$$

Finally, Y can be rendered inactive by a process assumed to follow first order kinetics,

$$Y \xrightarrow{\lambda_3} Y_i. \tag{10}$$

In summary, the reaction network from which the two corresponding models are derived consists of reactions (1)–(10). Species notation is summarized in Table I and the values of the kinetic constants and other parameters are shown in Table II. In the following, we will first analyze the behavior of the deterministic model, showing the two different types of oscillations that can be exhibited as well as the effect of growth and DNA production. Subsequently, we will investigate the effects of extrinsic and intrinsic stochasticity. To isolate the effects of intrinsic stochasticity, originating from small numbers of molecules, we will initially assume that the total operator DNA and the cellular volume remain constant. Subsequently, we will incorporate cell growth, DNA duplication, and division in order to investigate the effects of these extrinsic noise sources.

III. DETERMINISTIC MODELS

The deterministic model consists of the mass balances for the interacting species subject to conservation conditions. Concentration of species X is denoted as [X] (for species notation, see Table I). Since the operator exists in a free form as well as bound to the activator dimer and the total operator concentration, denoted $[O]_T$, is constant, the following conservation equation holds:

$$[O]_T = [O] + [OX_2]. \tag{11}$$

Furthermore, the total (active and inactive) degrader concentration, denoted $[Y]_T$, is also constant,

$$[Y]_T = [Y_i] + [Y]. \tag{12}$$

Utilizing the above relations and assuming that mass action kinetics apply to all reactions of the network the mass bal-

TABLE II. Parameters of the oscillator model.

Symbol	Value	Units	Description
V	14×10^{-15}	L	Volume[a]
O_T	2	(Copy number)	Total operator content (thus, $[O]_T\approx0.237$ nM)
Y_T	300	(Copy number)	Total degrader content (thus, $[Y]_T\approx35.6$ nM)
k_0	$0.075\cdot\zeta$	min^{-1}	Constitutive expression rate of X[b]
k_1	$140\cdot\zeta$	min^{-1}	Enhanced transcription rate of X[b]
k_2	0.014	$nM^{-1}\ min^{-1}$	Rate constant for activation of Y_i from X_2
χ	50	$nM^{-1}\ min^{-1}$	X dimerization rate constant
β	36	nM	X dimerization dissociation constant
ϕ	20	$nM^{-1}\ min^{-1}$	X_2-operator binding rate constant
α	22	nM	X_2-operator dissociation constant
λ_1	$0.0144\cdot\zeta$	$nM^{-1}\ min^{-1}$	Induced degradation rate constant for X[b]
λ_2	$0.0072\cdot\zeta$	$nM^{-1}\ min^{-1}$	Induced degradation rate constant for X_2 [b]
λ_3	0.002	min^{-1}	Y deactivation rate constant
ζ	[c]	(Dim/less)	Parameter controlling timescale separation

[a]The volume was taken to be that of a yeast cell with a representative diameter of approximately 3 μm.
[b]The value of these parameters affects timescale separation. Larger ζ values result in positive feedback being faster than the negative.
[c]For simulations where timescale separation exists, $\zeta=10$. For simulations where timescale separation is absent, $\zeta=1$.

ances for each of the four participating species are written as

$$\frac{d[O]}{dt} = -\phi\cdot[O]\cdot[X_2] + \alpha\cdot\phi\cdot([O]_T - [O]), \tag{13}$$

$$\frac{d[X]}{dt} = k_0\cdot[O] + k_1\cdot([O]_T - [O]) - 2\cdot\chi\cdot[X]^2 + 2\cdot\beta\cdot\chi\cdot[X_2] - \lambda_1\cdot[X]\cdot[Y], \tag{14}$$

$$\frac{d[X_2]}{dt} = -\phi\cdot[O]\cdot[X_2] + \alpha\cdot\phi\cdot([O]_T - [O]) + \chi\cdot[X]^2 - \beta\cdot\chi\cdot[X_2] - \lambda_2\cdot[X_2]\cdot[Y], \tag{15}$$

$$\frac{d[Y]}{dt} = k_2\cdot[X_2]\cdot([Y]_T - [Y]) - \lambda_3\cdot[Y]. \tag{16}$$

A. Bifurcation structure

In order to elucidate the behavior of our oscillator as predicted by the deterministic model, we first performed continuation simulations using XPPAUT (Ref. 33) of both steady states and periodic solutions of Eqs. (13)–(16). The main bifurcation parameter was chosen to be the dissociation constant α for the binding of the activator dimer to the operator, since it quantifies an important effect, namely, the strength of the positive feedback.

Furthermore, parameter ζ, appearing in the values of kinetic rates k_0, k_1, λ_1, and λ_2, quantifies the timescale separation between the positive and negative feedbacks as it affects the order of magnitude of the rates of production and degradation of the X species,

$$k_0 = 0.075\cdot\zeta, \quad k_1 = 140\cdot\zeta, \quad \lambda_1 = 0.0144\cdot\zeta, \quad \lambda_2 = 0.0072\cdot\zeta. \tag{17}$$

Figure 2(a) shows a bifurcation diagram for the parameter set of Table II with $\zeta=10$, which corresponds to faster positive versus negative feedback action [refer to Eq. (17) and Table II]. Notice that the system exhibits oscillations that have approximately constant amplitude for an extended range of the main bifurcation parameter α. On the other hand, Fig. 2(b) shows a qualitative different behavior in which the timescale of the positive feedback is comparable to that of the negative feedback loop ($\zeta=1$). In this case, the oscillations have smaller amplitude whose dependence on parameter α is much stronger than that of the previous case. On the other hand, in both cases, the oscillations emerge through an infinite period bifurcation that generates a homoclinic orbit at around $\alpha=14$ nM, and disappear at Hopf points close to $\alpha=26$ nM. Note also that the region of the parameter space where oscillations are observed remains practically the same.

The timescale separation not only affects the qualitative characteristics of the oscillations; it also influences whether the lower steady state (for high α values) will be excitable.[34] Panels (c) and (d) of Fig. 2 show the response of the system when a stimulus in X has been imposed as a square pulse in time,

$$\frac{d[X]}{dt} = f([O],[X],[X_2],[Y]) + A\cdot(H(t-t_1) - H(t-t_1-\Delta)), \tag{18}$$

where $f([O],[X],[X_2],[Y])$ is the right-hand side of Eq. (14), $H(\cdot)$ is the Heaviside unit step function, A is the amplitude and Δ the duration of the pulse, and t_1 is the time when the stimulus is imposed. In the case of significantly

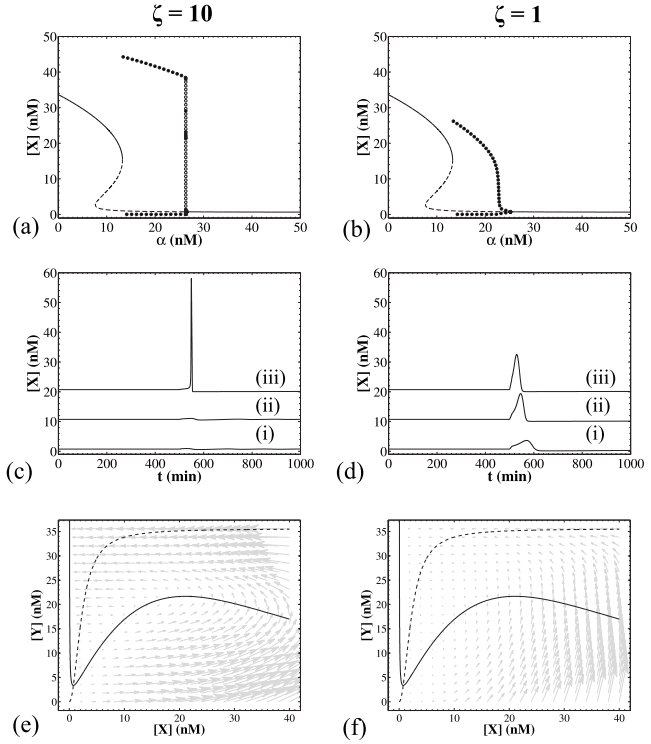

FIG. 2. Panels (a) and (b): bifurcation diagrams for species X in the cases where timescale separation exists (a, $\zeta=10$), and in the case where it is absent (b, $\zeta=1$). Solid lines represent stable steady states and dashed lines the unstable ones. Closed circles represent stable limit cycles and open circles the unstable ones. Panel (c): excitable behavior for $\zeta=10$, $\alpha=27$. Three transient simulations are shown, in which the system is initialized from the steady state and at $t_1=500$ min, square pulses with various amplitudes A and fixed duration $\Delta=10$ min are imposed on species X: (i) A=0.014 nM/min, (ii) A=0.015 nM/min, (iii) A=0.016 nM/min. For clarity, trajectories (ii) and (iii) are shifted +10 nM and +20 nM, respectively. Panel (d): as in panel (c) but with no timescale separation, $\zeta=0.1$. The amplitudes of the pulses in this case are (i) A=0.1 nM/min, (ii) A=0.2 nM/min, and (iii) A=0.4 nM/min. Panels (e) and (f): nullclines and vector fields for the reduced system (19)–(21) in the two cases (e, $\zeta=10$) and (f, $\zeta=1$). The solid line corresponds to the nullcline $d[X]/dt=0$ and the dashed one to $d[Y]/dt=0$. Parameters not mentioned have the values shown in Table II.

faster positive feedback loop dynamics [Fig. 2(c)] it is apparent that for stimuli slightly above a certain threshold, the response of the system is disproportionately large in comparison to the stimulus. This behavior is indicative of excitability, which is in contrast to the graded response observed in Fig. 2(d) where the positive feedback dynamics evolve on a timescale similar to that of the negative feedback loop.

B. Model reduction

Bifurcation structures and threshold phenomena similar to what has just been discussed were first investigated in models of neuronal excitation.[35–37] These dynamical systems can be described by two variable models in which the fast variable exhibits an S-shaped nullcline and the slow variable has a monotonic nullcline. A prototype such system characterized by a cubic nullcline for the activator and a linear one for the inhibitor is known as the FitzHugh–Nagumo system.[38–40] In order to verify whether our system exhibits such a topological structure we employed singular perturbation arguments (see Sec. 1 of the supplementary material[49]) to reduce the four-variable model (13)–(16) to the following two-variable model:

$$\frac{d[X]}{dt}=\psi([X])\cdot\left([O]_T\cdot\frac{k_0\cdot\alpha+k_1\cdot\frac{[X]^2}{\beta}}{\alpha+\frac{[X]^2}{\beta}}-\lambda_1\cdot[X]\cdot[Y]-2\cdot\lambda_2\cdot\frac{[X]^2}{\beta}\cdot[Y]\right), \tag{19}$$

$$\frac{d[Y]}{dt}=k_2\cdot\frac{[X]^2}{\beta}\cdot([Y]_T-[Y])-\lambda_3\cdot[Y], \tag{20}$$

where

$$\psi([X])=\frac{1}{1+4\cdot\frac{[X]}{\beta}\cdot\left(1+\frac{\alpha\cdot[O]_T}{\left(\alpha+\frac{[X]^2}{\beta}\right)^2}\right)}. \tag{21}$$

The nullclines and the vector fields of this model (19)–(21) in the presence or absence of timescale separation are shown in Figs. 2(e) and 2(f). We observe that the nullcline of the activator species X indeed exhibits an S-shaped structure. In the presence of large timescale separation, this branch acts as separatrix: $d[X]/dt>0$ and $d[Y]/dt\approx0$ immediately to the right of the branch, whereas $d[X]/dt<0$ and $d[Y]/dt\approx0$ to the left (panel e). Thus, if the system surpasses the separatrix, a large departure from the steady state will be observed, indicative of excitability (see panel c). On the other hand, if no timescale separation exists, $d[Y]/dt>0$ to the right of the branch and thus the inhibitory feedback is immediately triggered preventing the system from deviating far away from the steady state.

C. Effect of cell growth

Equations (11)–(16) neglect cell growth and division. In order to incorporate these effects, we formulate a continuum model[31,41] assuming that single cell growth is exponential[42] and that during cell growth, free operator DNA (species O) and inactive Y protein (species Y_i) are continuously produced, so that the conservation Eqs. (11) and (12) hold. We further assume that upon cell division, the concentrations of the mother and daughter cells are the same; thus, the equations for the species concentrations do not contain any terms pertaining to division (refer to Stamatakis[41] for more details) Then, if g is the growth rate parameter defined as

$$g=\frac{1}{V}\cdot\frac{dV}{dt}, \tag{22}$$

the deterministic continuum model that takes into account cell growth is written as (refer to Sec. 2 of the supplementary material for a detailed derivation)

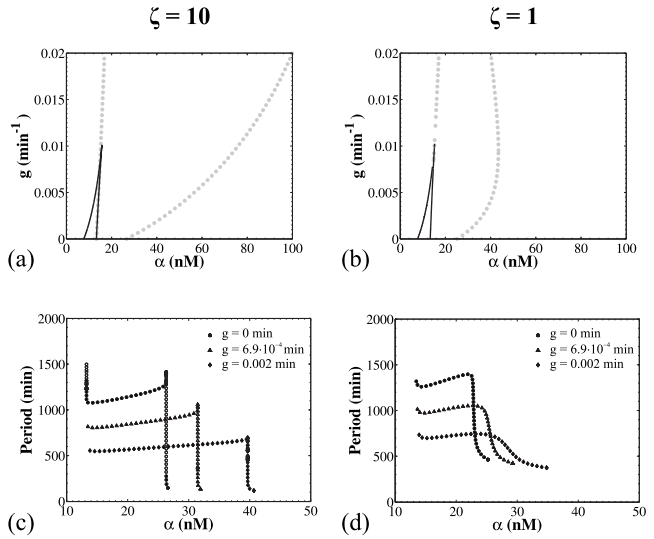

FIG. 3. Effect of growth on the bifurcation structure [panels (a) and (b)] and the periods [(c) and (d)] of the deterministic system [Eqs. (22)–(26)]. For panels (a) and (c) $\zeta=10$ and for (b) and (d) $\zeta=1$. Parameters not mentioned have the values shown in Table II.

$$\frac{d[O]}{dt} = -\phi\cdot[O]\cdot[X_2] + \alpha\cdot\phi\cdot([O]_T - [O]) + g\cdot([O]_T - [O]), \quad (23)$$

$$\frac{d[X]}{dt} = k_0\cdot[O] + k_1\cdot([O]_T - [O]) - 2\cdot\chi\cdot[X]^2 + 2\cdot\beta\cdot\chi\cdot[X_2] - \lambda_1\cdot[X]\cdot[Y] - g\cdot[X], \quad (24)$$

$$\frac{d[X_2]}{dt} = -\phi\cdot[O]\cdot[X_2] + \alpha\cdot\phi\cdot([O]_T - [O]) + \chi\cdot[X]^2 - \beta\cdot\chi\cdot[X_2] + -\lambda_2\cdot[X_2]\cdot[Y] - g\cdot[X_2], \quad (25)$$

$$\frac{d[Y]}{dt} = k_2\cdot[X_2]\cdot([Y]_T - [Y]) - \lambda_3\cdot[Y] - g\cdot[Y]. \quad (26)$$

In order to elucidate the effect of cell growth, we performed two parameter continuation studies of the above Eqs. (23)–(26) using XPPAUT.[33] The main bifurcation parameter was taken to be the OX_2 dissociation constant α, and the secondary parameter was the growth rate g. Panels (a) and (b) of Fig. 3 show the two parameter bifurcation diagrams for the cases where timescale separation exists or not, respectively. The black lines denote turning points and the closed gray circles Hopf points. In both cases, higher growth rates result in loss of the sigmoidal shape of the bifurcation, as evidenced by the vanishing of the turning points at approximately $g=0.01\ \text{min}^{-1}$. The latter value corresponds to a division time of around 70 min. This can be seen as a damping effect that destroys the bistable behavior of the system due to the dilution of the activator protein X.

On the other hand, cell growth has a nonintuitive effect in the Hopf points. One would expect that the damping effect just noted would also result in shrinkage of the parameter region where oscillations are observed. Contrary to intuition, this region is shown to extend for growth rates ranging from 0 to 0.02 min^{-1} for the system that exhibits timescale separation [Fig. 3(a)]. The oscillatory region assumes its maximum extent around $g=0.05\ \text{min}^{-1}$ after which it starts to shrink (not shown). If timescale separation is absent, the extent of the oscillatory region reaches a maximum around $g=0.01\ \text{min}^{-1}$ [Fig. 3(b)]. Such an effect could be stemming from either a strengthening of the positive feedback loop or a weakening of the negative one. Clearly, strengthening is not occurring, since species X, X_2 are subject to dilution during cell growth, and the operator produced is in the unbound state. Thus, it seems that the dilution of species Y weakens the negative feedback, thereby allowing the oscillations to occur even for higher dissociation constants α. Of course, this effect is only observed for relatively slow growth, as for much higher growth rates the dilution of the activator species and the bound operator result in the shrinking of the oscillatory region.

As far as the periods of the oscillations are concerned, panels (c) and (d) of Fig. 3 reveal that higher growth rates result in lower periods for both cases where timescale separation exists or is absent. This trend is not limited to the values of g shown in these plots, but persists for virtually the entire range of growth rates for which oscillations are observed. This effect could be explained as a rescaling of time in Eqs. (23)–(26). By applying the transformation $t^*=g\cdot t+c$, the effect of growth is absorbed in the time variable and dimensionless kinetic rates appear in the right-hand side of these equations. Assuming that the period of the dimensionless system changes slower than the value of g, one would expect that higher growth rates result in a decrease in the period of the dimensional system.

IV. STOCHASTIC MODELS

The simulations that we described so far showed that the system, as defined by the specific set of reactions, does or does not exhibit excitability and sharp oscillations, depending on the relative magnitude of the timescales in which the positive and negative feedback loops evolve. These simulations, performed with the deterministic model, completely neglect stochasticity. However, cellular systems contain small numbers of molecules in volumes to the order of femtoliters, thereby making stochasticity considerable. Thus, it is necessary to investigate the behavior of the system under the influence of stochastic fluctuations, in the presence or absence of timescale separation.

A. Intrinsic noise

The stochastic model that accounts for intrinsic noise stemming from stochasticity in reaction occurrence is the chemical master equation[32]

$$\frac{\partial P(\mathbf{x},t|\mathbf{x}_0,t)}{\partial t} = \sum_{j=1}^{m}[a_j(\mathbf{x}-\mathbf{v}_j)\cdot P(\mathbf{x}-\mathbf{v}_j,t|\mathbf{x}_0,t) - a_j(\mathbf{x})\cdot P(\mathbf{x},t|\mathbf{x}_0,t)]. \quad (27)$$

For our system, the master equation is impossible to solve analytically, and thus, we used the Gillespie algorithm[32,43] to simulate stochastic paths that follow Eq. (27). The state vec-

TABLE III. Propensity functions for the oscillator model.

	Reaction	Propensity function[a–c]
(1)	$O \xrightarrow{k_0} O+X$	$a_1 = k_0 \cdot O$
(2)	$2X \xrightarrow{\chi} X_2$	$a_2 = \frac{\chi}{V \cdot N_A} \cdot X \cdot (X-1)$
(3)	$X_2 \xrightarrow{\beta\chi} 2X$	$a_3 = \beta \cdot \chi \cdot X_2$
(4)	$O+X_2 \xrightarrow{\phi} OX_2$	$a_4 = \frac{\phi}{V \cdot N_A} \cdot X_2 \cdot O$
(5)	$OX_2 \xrightarrow{\alpha\phi} O+X_2$	$a_5 = \alpha \cdot \phi \cdot OX_2$
(6)	$OX_2 \xrightarrow{k_1} OX_2+X$	$a_6 = k_1 \cdot OX_2$
(7)	$Y_i+X_2 \xrightarrow{k_2} Y+X_2$	$a_7 = \frac{k_2}{V \cdot N_A} \cdot X_2 \cdot Y_i$
(8)	$X+Y \xrightarrow{\lambda_1} Y$	$a_8 = \frac{\lambda_1}{V \cdot N_A} \cdot X \cdot Y$
(9)	$X_2+Y \xrightarrow{\lambda_2} Y$	$a_9 = \frac{\lambda_2}{V \cdot N_A} \cdot X_2 \cdot Y$
(10)	$Y \xrightarrow{\lambda_3} Y_i$	$a_{10} = \lambda_3 \cdot Y$

[a]Variables without brackets denote number of molecules of the corresponding species.
[b]All propensity functions have units of min^{-1}.
[c]Avogadro's number: $N_A = 6.022\,136\,7 \times 10^{14}$ nmol^{-1}.

tor containing numbers of molecules for each species is $\mathbf{x} = \{O, X, X_2, OX_2, Y_i, Y\}$, and we have $n=6$ species participating in $m=10$ reactions. The reactions' propensity functions, $a_j(\mathbf{x}) = c_j \cdot h_j(\mathbf{x})$, $j = 1, 2, \ldots, m$, can be calculated given the macroscopic kinetic constants of Table II, and are presented in Table III. The vectors v_j denote the change in the number of molecules for each species, e.g., for reaction (4), $v_4 = \{-1, 0, -1, 1, 0, 0\}$.

The predictions of the stochastic model must agree with those of the deterministic model for infinitely large systems (system size expansion[44]). The system size is quantified by extensive variables, namely, the volume (V) in which the reactions take place and the number of molecules of the conserved species (O_T and Y_T, respectively). These parameters appear in the propensity functions of the master Eq. (27). On the contrary, in the deterministic model, the numbers of molecules of the conserved species exist only in their intensive form as concentrations (intensive variables). To ensure the validity of the comparison between the deterministic and stochastic models, the concentrations of the conserved species ($[O]_T, [Y]_T$) were kept fixed at the same values in both types of simulations, whereas the volume (V) was used to study the effect of system size in the case of stochastic simulations. To validate our comparative approach, test simulations were run for very large system sizes. As expected, the stochastic model effectively exhibits deterministic behavior, since the effect of stochastic fluctuations becomes practically negligible (Fig. 4).

TABLE IV. Division cycle parameters.

Symbol	Value	Units	Description
g	[a]	min^{-1}	Growth rate
$V_{dup,crit}$	14×10^{-15}	L	Critical DNA duplication volume
n_{dup}	25	(Dim/less)	DNA duplication sharpness parameter
$V_{div,crit}$	14×10^{-15}	L	Critical cell division volume
n_{div}	25	(Dim/less)	Cell division sharpness parameter
q	80	(Dim/less)	Daughter size variation parameter

[a]The growth rate was varied, so that the cell division times range from 1 h to 3 days, in order to investigate the interplay between division cycle and oscillatory response.

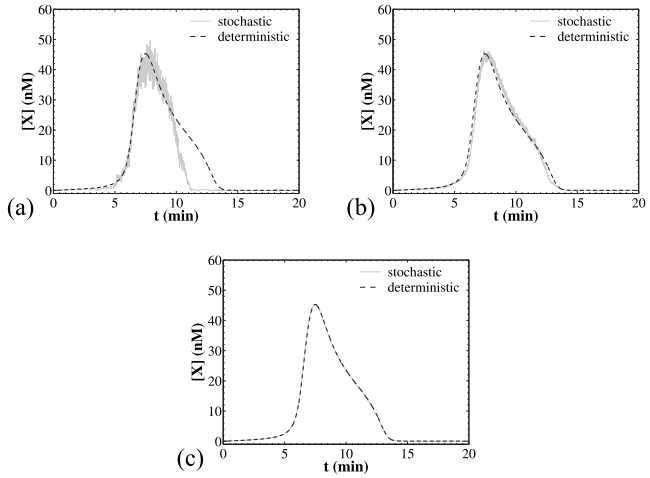

FIG. 4. Comparison of stochastic with deterministic trajectories as the system size increases. Panel (a): $V = 7 \times 10^{-15}$ L, copy numbers for conserved species $O_T = 1$, $Y_T = 150$. Smallest possible system size (single operator), significant stochasticity. Panel (b): $V = 84 \times 10^{-15}$ L, copy numbers for conserved species $O_T = 12$, $Y_T = 1800$. Lower noise strength. Panel (c): $V = 15\,771 \times 10^{-15}$ L, copy numbers for conserved species $O_T = 2253$, $Y_T = 337\,950$. Effectively deterministic behavior. All other parameter values as in Table II with $\zeta = 10$, $\alpha = 20$ nM.

Thus, we will use this comparative approach to study the effect of stochasticity on the oscillation characteristics, in the far more interesting case of biologically relevant, smaller system sizes. In deterministic models periodicity can be easily determined from the requirement that there exists a real number T (the period) such that $\mathbf{x}(t+n \cdot T) = \mathbf{x}(t)$, $\forall n \in \mathbb{Z}$. In the stochastic model periodicity is determined in a statistical sense using the autocovariance function (κ_Y) and the spectral density function (S_Y). The former is defined as[44]

$$\kappa_Y(\tau) := \langle (Y_t - \langle Y_t \rangle) \cdot (Y_{t+\tau} - \langle Y_{t+\tau} \rangle) \rangle, \tag{28}$$

whereas the latter is the Fourier transform of the autocovariance function according to the Wiener–Khinchin theorem.[44] Since the autocovariance function is even for stationary processes, it suffices to take a cosine transformation of the former to compute the spectral density,

$$S_Y(\omega) = 2 \cdot \int_0^\infty \kappa_Y(\tau) \cdot \cos(\omega \cdot \tau) d\tau. \tag{29}$$

According to the theory of stochastic processes,[45] when a stochastic signal has periodic components, the autocovariance function exhibits oscillatory patterns [Fig. 5(a)] and, consequently, peaks are observed in the spectral density function [Fig. 5(b)]. We note that in the simple case of a single periodic component, one can observe multiple peaks that correspond to the component's harmonic frequencies

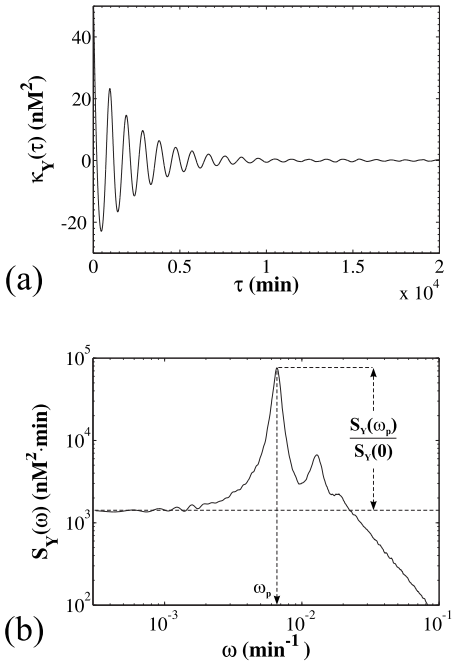

FIG. 5. Panel (a): typical autocovariance function for a stochastic oscillation. Panel (b): typical spectral density for a stochastic oscillation. The preferred frequency is denoted ω_p. Parameter values as in Table II with $\zeta=10$, $\alpha=20$ nM.

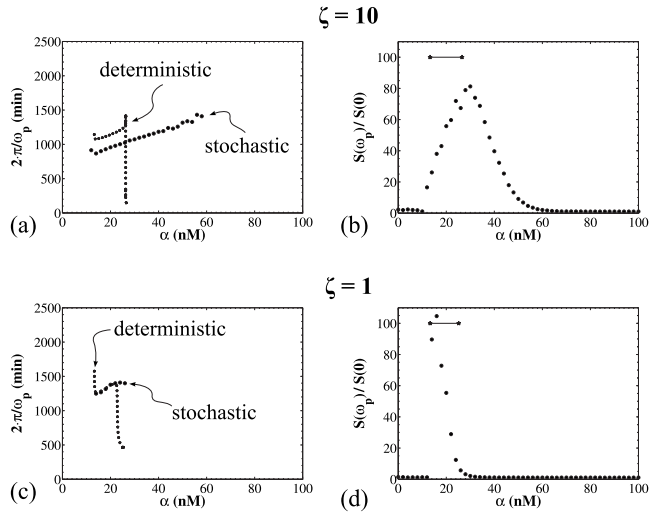

FIG. 6. Panel (a): consistency of the oscillations as quantified by the ratio $S(\omega_p)/S(0)$. Marked with ★–★ is the deterministic oscillatory region. Panel (b): preferred periods of the stochastic oscillations in comparison to the deterministic periods. Parameters as in Table II with $\zeta=10$. Panels (c) and (d): as in panels (a) and (b) but for the case where no timescale separation exists and no excitability was observed deterministically (parameters as in Table II with $\zeta=1$).

(integer multiples of a base frequency). Further, note that the fastest the decay of the autocovariance, the more quickly the oscillations desynchronize and the less pronounced the maximum of the spectral density. We will thus quantify the *consistency* of the oscillations with the ratio $S_Y(\omega_p)/S_Y(0)$. More consistent oscillations have higher $S_Y(\omega_p)/S_Y(0)$ ratios and desynchronize slower than less consistent oscillations. Thus, for each parameter set we were able to determine whether our system exhibits stochastic oscillations or not by detecting the presence of at least one maximum with $S_Y(\omega_p)/S_Y(0)>2$ in the spectral density. The frequency for which the first maximum is found will be referred to as the preferred frequency ω_p and the corresponding period as the preferred period ($T_p=2\times\pi/\omega_p$).

B. Effect of noise and timescale separation on oscillation characteristics

Following the methodology and using the tools discussed in Sec. IV A we can now compare in a meaningful way the deterministic and stochastic models. For systems to the order of a yeast cell (diameters of 3–4 μm; V $\approx$14–34 fL), stochastic fluctuations can profoundly affect the behavior of the system. Such effects are shown in Fig. 6, which depicts simulation results corresponding to the parameter set for which excitability was observed in the deterministic model ($\zeta=10$). In panel (a) the ratios $S(\omega_p)/S(0)$ quantifying the consistency of the oscillations are shown. Notice that the range of O-X_2 dissociation constant α for which stochastic oscillations are observed is significantly larger than that of the deterministic model. Moreover, stochastic oscillations are exhibited not only in the deterministically oscillatory region, but also in the deterministically excitable region. The oscillations in the latter region can be thought as emanating from stochastic stimulation of the excitable steady state: the system continuously fluctuates around this steady state when, at some point in time, a large enough fluctuation (superthreshold stimulus) excites the system. The system temporarily "departs" far away from the excitable state but after some characteristic recovery time it approaches the excitable state again. Once this cycle has been completed, the system is ready to get reexcited. This series of excitations manifests as a stochastic oscillation in the region where only one excitable state is observed deterministically. This behavior is indicative of coherence resonance for our system.

Furthermore, Fig. 6(b) shows the preferred periods $2\cdot\pi/\omega_p$ of the stochastic oscillations in comparison to the periods of the deterministic oscillations. Interestingly, the former are significantly lower than the latter; thus, for this case, stochasticity seems to accelerate the pace of the oscillations. This observation can be explained by the underlying mechanism that generates the oscillations in this reaction network. For this parameter set in the deterministic model, the onset of a cycle is brought about by the fast autocatalytic action of species X, once the concentrations of species Y has dropped significantly, thereby weakening the negative feedback. However, for the stochastic model, the random fluctuations can fire the autocatalytic action of species X, even when the concentration of species Y is still relatively high. Consequently, the onset of a next cycle in the stochastic oscillation occurs prematurely in comparison to the deterministic case, and thus the preferred periods of the stochastic oscillations are lower than the deterministic case.

Hence, we have demonstrated that for the parameter set that results in large timescale separation (and for which excitability is observed deterministically), stochasticity results in broadening the oscillatory region and accelerating the

pace of the oscillations. This is not the case, however, for the parameter set where no excitability is exhibited deterministically.

In the latter case, the region where stochastic oscillations are exhibited is essentially the same as the oscillatory region of the deterministic model [Figs. 6(c) and 6(d)]. Note that the noise strength has not changed from the previous case, since the system size was kept the same. Yet, for this parameter set, the steady state is not excitable, and therefore, it cannot be stimulated by the stochastic fluctuations in order to produce robust stochastic oscillations. Thus, no broadening of the oscillatory region is observed.

Furthermore, as shown in Fig. 6(d), the preferred periods of the stochastic oscillations are very close to the deterministic periods. This result can be attributed to the fact that for this parameter set the positive and negative feedbacks proceed at approximately the same timescale. Therefore, the dynamics of the activating species X are as slow as those of the degrader species Y, and thus X cannot exert the autocatalytic feedback fast enough in order to prematurely initiate the next cycle of the oscillation.

C. System size expansion

All previously presented results were obtained for a certain system size similar to that of a typical yeast cell size. However, it is interesting to investigate the effect of noise strength on the existence and the properties of the oscillations. As we have already shown, for very large systems, the predictions of the stochastic model agree with those of the deterministic model. Thus, the stochastic oscillations that are exhibited in the deterministically oscillatory regions will progressively become more consistent and for infinite system sizes, the autocovariance will follow a nondecaying oscillatory pattern. This effect is confirmed by simulations (results not shown).

By the same token, the oscillations exhibited in the deterministically excitable region (for the parameter set where $\zeta=10$) are expected to vanish for some large system size. Before vanishing, however, an interesting nonlinear effect is observed [Figs. 7(a), 7(c), and 7(d)]: for progressively larger system sizes, the oscillations initially become more and more consistent until a critical system size from which the oscillations start becoming less consistent until they vanish. This effect can be explained as follows: it is known that the noise strength decreases for increasing system sizes due to averaging of the stochastic fluctuations.[46] Small fluctuations are ineffective in exciting the system in a periodic fashion, since the noisy jumps are rarely strong enough to surpass the threshold, as shown in panel (f) where the nullclines of the reduced deterministic model are plotted along with the stochastic trajectory. Thus, the oscillations must become less consistent as the system size increases. On the other hand, lower noise results in higher regularity in the duration of the excursions from the excitable steady state. Thus, from this perspective, for larger system sizes the oscillations should become more consistent as the timing of the return to the steady state for reexcitation becomes more precise.

These two conflicting factors shape the behavior of the system as follows: for small system sizes, oscillations are

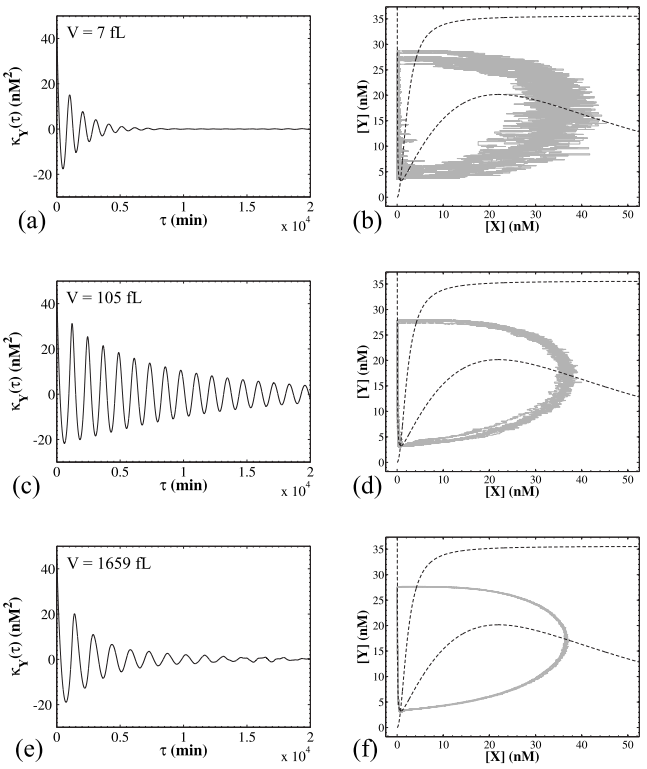

FIG. 7. Nonlinear effect of the noise strength on the robustness of stochastic oscillations exhibited in the deterministically excitable region. Panel (a): $V=7\times10^{-15}$ L, copy numbers for conserved species $O_T=1$, $Y_T=150$. Panel (b): nullclines of the reduced deterministic model (19)–(21) and trajectory of the stochastic model on the [X], [Y] plane. Panels (c) and (d): $V=105\times10^{-15}$ L, copy numbers for conserved species $O_T=15$, $Y_T=2250$. Panels (e) and (f): $V=1659\times10^{-15}$ L, copy numbers for conserved species $O_T=237$, $Y_T=35\,550$. All other parameter values as in Table II with $\zeta=10$, $\alpha=30$ nM.

observed but they are not quite consistent, since the excursion times have a large variability. Larger system sizes result in more consistent oscillations due to the regularity of the excursions, as long as the noise strength is still high enough to be able to excite the system. However, for much larger systems, the noise strength becomes significantly lower, so that excitation becomes incoherent and the oscillations start becoming less consistent. This biphasic effect is essentially a coherence resonance phenomenon,[20] according to which moderate but not very high or very low noise magnitudes lead to maximal coherence of the noise-induced oscillations.

D. Extrinsic noise: Incorporation of growth, DNA duplication, and division

The stochastic model discussed so far neglects cell growth and division. The latter effects were investigated in the deterministic case, under the assumptions that DNA production occurs continuously and that the concentrations of mothers and daughters are the same upon division. We wish to investigate these effects in the stochastic case as well, noting that neither of these assumptions hold true anymore. Rather, DNA production will be considered as a discrete event in which the number of operators is doubled. New operators are produced in the unbound state. Furthermore,

upon partitioning, each mother cell will inherit two operator DNA molecules with random state (free or bound) that follows a hypergeometric distribution. All other species are partitioned according to a binomial distribution. Cell growth is incorporated as a deterministic time-dependency in the propensity functions[47] and the total concentration $[Y]+[Y_i]$ is kept approximately constant around the value $[Y]_T$ by producing single Y_i molecules at specific times. Finally, the single cell master equation incorporating growth DNA duplication and division has the general form,[48]

$$\frac{\partial P(\mathbf{x},V,t)}{\partial t} = \sum_{j=1}^{m} [a_j(\mathbf{x}-\mathbf{v_j},V)\cdot P(\mathbf{x}-\mathbf{v_j},V,t) - a_j(\mathbf{x},V)\cdot P(\mathbf{x},V,t)] + a_Y(Y_i,Y,V)\cdot P(\mathbf{x}-\mathbf{v_Y},V,t) - a_Y(Y,V)\cdot P(\mathbf{x},V,t)$$
$$+ a_{dup}(\mathbf{x}-\mathbf{v}_{dup},V)\cdot P(\mathbf{x}-\mathbf{v}_{dup},V,t) - a_{dup}(\mathbf{x},V)\cdot P(\mathbf{x},V,t) - \frac{\partial}{\partial V}[g\cdot V\cdot P(\mathbf{x},V,t)]$$
$$+ \sum_{k_1\geq 0}\cdots\sum_{k_n\geq 0}\int_0^{\infty} a_{div}(\mathbf{x}+\mathbf{k},V+\vartheta)\cdot h(\mathbf{x},V|\mathbf{X}+\mathbf{k},V+\vartheta)\cdot P(\mathbf{x}+\mathbf{k},V+\vartheta,t)d\vartheta - a_{div}(\mathbf{x},V)\cdot P(\mathbf{x},V,t). \quad (30)$$

The reaction propensity expressions that appear in the above equation are shown in Table III. The propensity for the production of a Y_i molecule, a_Y, is defined as

$$a_Y(Y,Y_i,V) = 0 \quad \text{for} \quad \frac{Y+Y_i+0.5}{N_A\cdot V} > [Y]_T,$$

$$a_Y(Y,Y_i,V) \to \infty \quad \text{for} \quad \frac{Y+Y_i+0.5}{N_A\cdot V} \leq [Y]_T, \quad (31)$$

and the vector of change $\mathbf{v_Y}=\{0,0,0,0,1,0\}$. The above expression results in the production of a Y molecule exactly when the total Y concentration drops below the desired $[Y]_T$ at some point in the lifetime of the cell (the 0.5 term in the numerator is a continuity correction). As a result, the total Y concentration fluctuates around the $[Y]_T$ value while the cell grows.

The vector of change for DNA duplication is $\mathbf{v_Y}=\{2,0,0,0,0,0\}$ and the propensity for this event is

$$a_{dup}(\mathbf{x},V) = \left(\frac{V}{V_{dup,crit}}\right)^{n_{dup}}\cdot \mathbf{1}_{\{O+OX_2=2\}}, \quad (32)$$

where $\mathbf{1}_{\{E\}}$ is an indicator variable that evaluates to 1 if E is true, and 0 otherwise. The above relation describes stochastic DNA duplication if the volume is close to $V_{dup,crit}$, provided that only two operator DNA molecules exist. As a result of the duplication event, two free operator molecules are produced inside the cell, thereby doubling the total number of operator molecules, $O_T=4$. Thus, DNA duplication is performed only once per division cycle. Parameter n_{dup} controls the sharpness of the duplication mechanism: for $n_{dup}\to\infty$ duplication takes place exactly the moment when $V(t)=V_{dup,crit}$. Finite values of n_{dup} allow for some variation in the size of the cell (and thus the time) when duplication occurs.

The convective term in Eq. (30) expresses cell growth under exponential single cell growth law. Hence, the volume of the cell between subsequent divisions is given as

$$\frac{dV}{dt} = g\cdot V. \quad (33)$$

Finally, the second to the last term expresses a probability influx due to division of mother cells with contents $x_i+k_i\geq x$, $i=1,\ldots,n$ and volumes $V+\vartheta>V$, and the last term is a probability efflux due to division of cells in state $(\mathbf{x},V)$. The division propensity is

$$a_{div}(\mathbf{x},V) = \left(\frac{V}{V_{div,crit}}\right)^{n_{div}}\cdot \mathbf{1}_{\{O+OX_2=4\}}, \quad (34)$$

and therefore division can occur when the volume is around $V_{div,crit}$ only if the total operator content is four molecules. The latter ensures that division always succeeds DNA duplication. Parameter n_{div} controls the sharpness of the division mechanism.

The function $h(\mathbf{x},V|\mathbf{X}+\mathbf{k},V+\vartheta)$ is the conditional probability of finding one daughter with contents $\mathbf{x}$ and volume V given that a daughter of contents $\mathbf{x}+\mathbf{k}$ and volume $V+\vartheta$. We use the following form for this probability:

$$h(\mathbf{x_d},V_d|\mathbf{x_m},V_m) = hg(O_d,OX_{2,d}|O_m,OX_{2,m}) \cdot \prod_{\substack{x_i\neq O \\ x_i\neq OX_2}} bn_i(x_{i,d}|x_{i,m},V_m,V_d)\cdot\beta(V_d|V_m), \quad (35)$$

in which the indices m and d denote mother cell and daughter cell, respectively. The above expression incorporates the assumptions of volume partitioning following a beta distribution:

$$\beta(V_d|V_m) = \frac{1}{V_m}\cdot\frac{\Gamma(2\cdot q)}{(\Gamma(q))^2}\cdot\left(\frac{V_d}{V_m}\right)^{q-1}\cdot\left(1-\frac{V_d}{V_m}\right)^{q-1}. \quad (36)$$

In the above expression, parameter q captures the variation of the cell size of the two daughters. For $q\to\infty$ the division

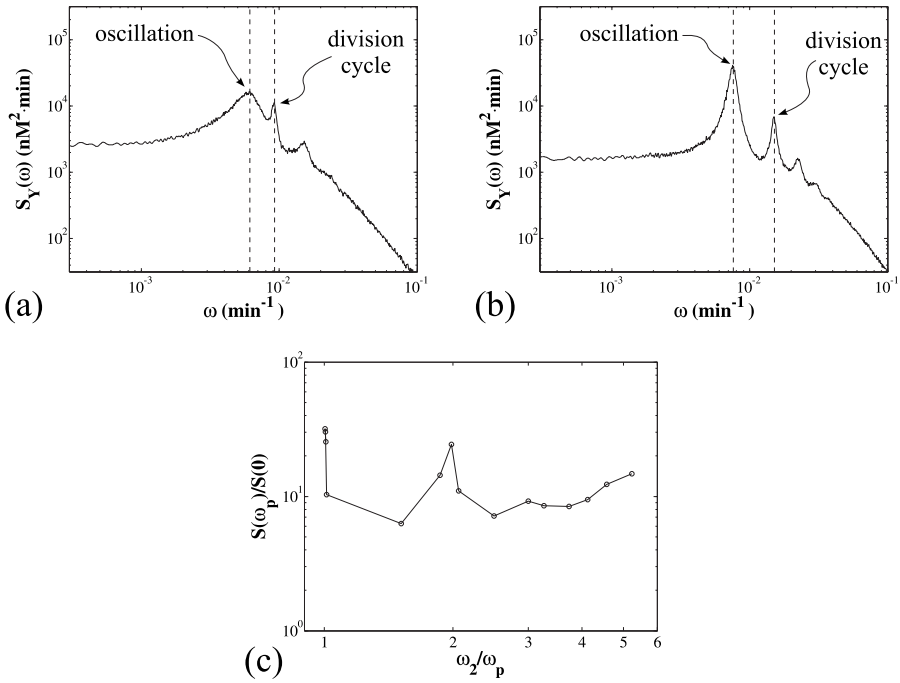

FIG. 8. Representative spectral density functions $S_Y(\omega)$ for the stochastic model that incorporates division cycle effects [Eqs. (30)–(38)]. Panel (a): $\zeta=1$, $\alpha=40$ nM, $g=0.001$ min^{-1}. The lower mode is at $\omega_p \approx 0.0061$ min^{-1} ($T_p \approx 1037$ min) and the high mode, which corresponds to the division cycle, at $\omega_2 \approx 0.0092$ min^{-1} ($\tau_2 \approx 680$ min). Panel (b): as in panel (a) but for $g=0.0017$ min^{-1}. The lower mode is at $\omega_p \approx 0.0075$ min^{-1} ($T_p \approx 836$ min) and the high mode at $\omega_2 \approx 0.0150$ min$^{-1}=2\cdot\omega_p$ ($\tau_2 \approx 418$ min). Panel (c): consistency of the oscillation with respect to the ratio between the division frequency and the preferred frequency of the oscillation. All other parameter values as in Tables II and IV.

is always symmetric; lower q values result in asymmetric division occurrences as well.

Furthermore, expression (35) incorporates binomial partitioning of non-DNA species x_i,

$$bn_i(x_{d,i}|x_{m,i},V_m,V_d)=\binom{x_{m,i}}{x_{d,i}}\cdot\left(\frac{V_d}{V_m}\right)^{x_{d,i}}\cdot\left(1-\frac{V_d}{V_m}\right)^{x_{m,i}-x_{d,i}}, \tag{37}$$

and partitioning of an operator DNA species that follows a hypergeometric distribution,

$$hg(O_d,OX_{2,d}|O_m,OX_{2,m})=\binom{O_m}{O_d}\cdot\binom{OX_{2,m}}{OX_{2,d}}\cdot\binom{4}{2}^{-1}. \tag{38}$$

E. Division cycle effects

The incorporation of growth, DNA duplication, and division on the stochastic model essentially introduces another source of periodicity, stemming from the division cycle. The preferred period of this cycle is equal to the doubling time of the cell,

$$\tau_2=\frac{2\cdot\pi}{\omega_2}=\frac{\ln(2)}{g}, \tag{39}$$

where ω_2 is the frequency of the division cycle. This source of periodicity could not be taken into account in the deterministic continuum model (23)–(26) because of the assumptions of continuous DNA production and equal concentrations in mother and daughter cells.

In Fig. 8(a), the spectral density of the concentration of species Y is shown to exhibit two prominent modes. The one at the lowest frequency corresponds to the oscillatory component of the system, and the high frequency mode to the division cycle. In this case, the two periodic components coexist without interference. On the other hand, when the division cycle is approximately two times faster than the oscillation (panel b), the modes corresponding to the frequency of the oscillation as well as higher harmonic frequencies become more prominent. This is a resonance effect between the oscillator and the division cycle, and is also shown in panel (c), where the consistency of the oscillations is plotted with respect to the ratio of the two frequencies ω_2 and ω_p. The maxima observed for $\omega_2=\omega_p$ and $\omega_2=2\cdot\omega_p$ are indicative of this resonance effect.

In order to further investigate the effect of the division cycle on the oscillations of the system, simulations of Eqs. (30)–(38) were performed for an extended range of growth rates. The results appear in Fig. 9, in which panels (a) and (b) and (c) and (d) correspond to the case where timescale separation is absent or exists, respectively. Plotted is the preferred period of the stochastic system in comparison with the period of the oscillation of the deterministic continuum model.

Panel (a) compares the periods of the two models in the case of no timescale separation and for a value of α for which the chemical master equation exhibits robust oscillations. For this case, the periods of both models are in good agreement up to the point that they become equal. Then, for division frequencies lower than the oscillation frequency, the spectral mode corresponding to the division cycle is higher than that of the oscillation, and thus the preferred period of the system appears to be the cell division time.

For a higher value of $\alpha=40$ nM (panel b), for which the chemical master equation was found unable to produce oscillations [see Fig. 6(c)], the stochastic model that incorporates the division cycle exhibits a robust oscillatory behavior. The consistency factors $S(\omega_p)/S(0)$ of the latter are on the order of 10–30, as previously shown in Fig. 8(c). Note that for this parameter set, the deterministic system also exhibits oscillations albeit in a narrower region of the parameter

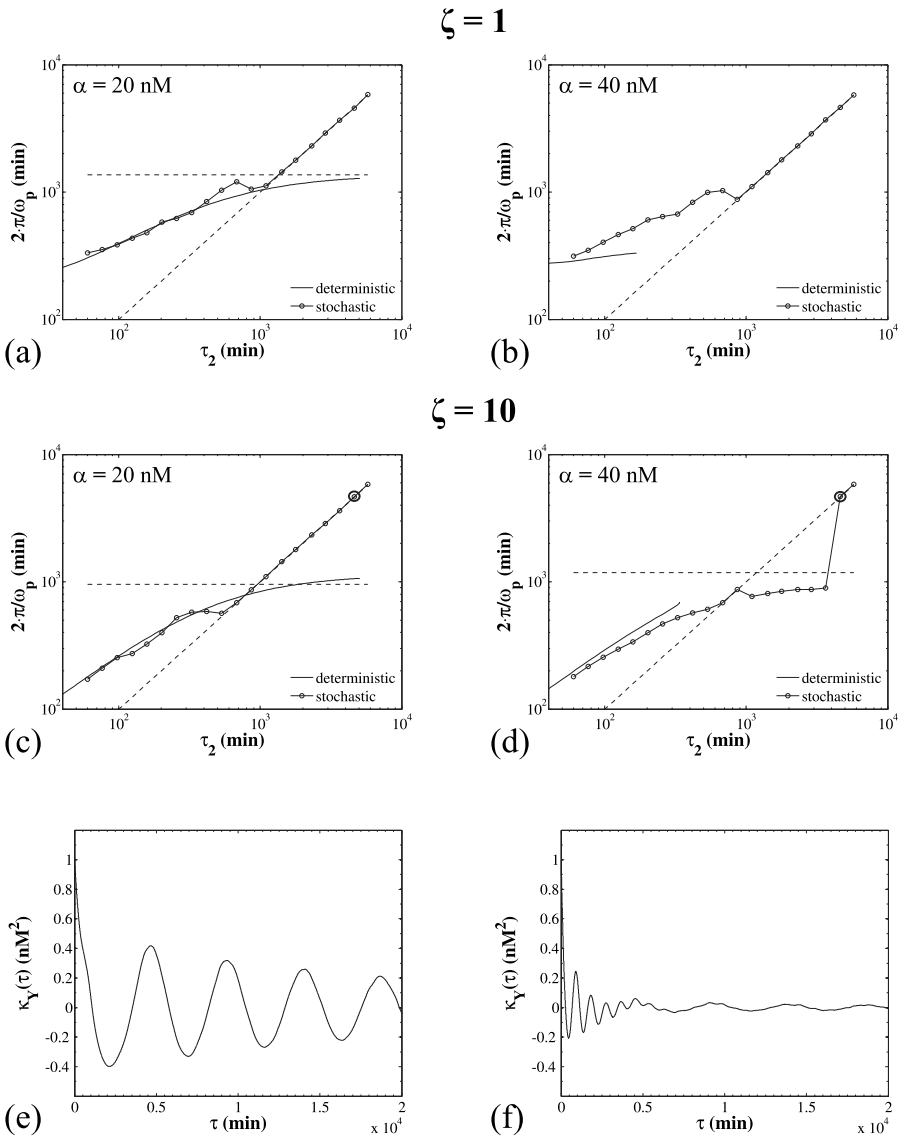

FIG. 9. Panels (a)–(d): effect of division cycle on the oscillations of the stochastic model [Eqs. (30)–(38)]. The preferred periods of the stochastic system are compared with the periods of the deterministic continuum model. The horizontal dashed line shows the preferred period of the stochastic system in the absence of growth, division, and DNA duplication [chemical master Eq. (27)]. This line is omitted when the chemical master equation does not exhibit oscillations. The inclined dashed line corresponds to $2\cdot\pi/\omega_p = \tau_2$. Panels (e) and (f): autocovariance functions for [Y] corresponding to the points marked in panels (c) and (d), respectively. Parameter values as noted; otherwise the values of Tables II and IV were used.

space ($\tau_2 < 200$ min). Thus, these oscillations result from stochastic sources associated with the division cycle alone.

In the case where timescale separation exists and both the continuum deterministic and the stochastic models oscillate (α=20 nM, panel c), we see that the periods of both models are in good agreement. This is in contrast to the case where no division cycle is accounted for [see Fig. 6(a)], where intrinsic noise was found to lower the period of the oscillation. For this case it is possible that the dilution due to cell growth inhibits the premature excitation of the system, and thus the period-lowering effect is no longer observed.

Finally, for a higher value of α=40 nM (panel d) the stochastic model is shown to exhibit oscillations for a much larger range of division times than the deterministic model: the oscillations of the latter cease to exist at a division time τ_2 around 300 min, and lower growth rates result in the deterministic system approaching a steady state. Moreover, the preferred periods of the stochastic model are again lower than those of the deterministic model. It is further interesting to observe that, in this case, the oscillatory mode in the spectral density is more prominent than the mode corresponding to cell division for a large region of the parameter space. The latter mode becomes more prominent for rather low growth rates, for which the autocovariance reveals the coexistence of two underlying frequencies (panel f): the oscillatory component of the reaction network appears to be superimposed on the periodic component due to cell division.

V. DISCUSSION

Aiming at investigating the effects of timescale separation, as well as intrinsic and extrinsic stochasticity on biological oscillations, we constructed a minimal reaction network which consists of a single positive coupled with a single negative feedback loop. The network is capable of exhibiting excitable or nonexcitable behavior. We subsequently derived corresponding deterministic and stochastic models that neglect the division cycle and models that incorporate cell growth, DNA production, and division, and compared their dynamical behaviors on the basis of (i) the extent of the parameter space where each model can exhibit oscillatory behavior and (ii) the properties of these oscillations. For the deterministic models, we performed the continuation of steady states and limit cycles to identify the oscillations

and their characteristics. For the stochastic models, the Gillespie algorithm and a variation thereof that incorporates growth, division, and DNA duplication was used to simulate the system. Subsequently, tools from the theory of stochastic processes (autocovariance and spectral density) were employed for detecting and analyzing the oscillations in the stochastic sense.

It was found that depending on the existence of timescale separation different behaviors can be observed as a result of the intrinsic noise. For large separation, simulations performed for system sizes to the order of a yeast cell showed that stochasticity greatly extends the oscillatory region and lowers the period. This behavior is in contrast to what was observed in the absence of timescale separation but for the same system size (and thus noise strength) as before. For this case, it was found that the stochastic oscillatory region is effectively identical to the deterministic one, and the preferred periods of the stochastic oscillations are very close to the deterministic periods.

Furthermore, the extension of the oscillatory region strongly depends on the noise strength as quantified by the system size. This effect was demonstrated by performing simulations in the presence of timescale separation, for a parameter set where the stochastic model oscillates but the deterministic does not. The following nonlinear result was thus observed: for increasing system sizes, the stochastic oscillations initially become more consistent, but after a critical system size they progressively lose consistency and finally vanish for much larger system sizes. This effect can be attributed to the interplay between noise strength and timing of the return to the steady state for reexcitation. For high to moderate noise (low to moderate system size) this timing becomes more precise, and thus, the consistency of the oscillation is improved. However, for lower noise (higher system size) the noise level decreases to the point that stochastic fluctuations are unable to reexcite the system in a consistent way, if at all. Such a biphasic effect is indicative of stochastic resonance.

On the other hand, intrinsic noise due to random reaction occurrence is not the only source of stochasticity in biological systems. The processes of cell growth, DNA duplication, and division are also stochastic and introduce extrinsic noise, the effects of which were investigated for our system. It was found that in the case of no timescale separation, for which intrinsic noise was unable to extend the oscillatory region, the extrinsic noise sources are able to do so for an extended range of growth rates. Furthermore, it was observed that the interplay between the division frequency and the frequency of the oscillation can result in resonance effects which strengthen the robustness of the oscillation.

These results show that intrinsic and extrinsic noise sources in synergy with timescale separation can enhance the robustness of the system, because they can increase the region where the desired behavior is observed. This effect could be physiologically significant, since vast timescale separation is indeed observed in many biological pathways. It is further possible that cells can tune the frequency of their division cycle with respect to that of a biological clock, or vice versa, in order to exploit resonance effects which also promote more robust oscillations.

ACKNOWLEDGMENTS

The financial support of NIH-NIGMS through Grant No. R01 GM071888 is gratefully acknowledged.

[1]P. L. Lakin-Thomas and S. Brody, Annu. Rev. Microbiol. **58**, 489 (2004).
[2]E. Carafoli, Proc. Natl. Acad. Sci. U.S.A. **99**, 1115 (2002).
[3]J. M. Mitchison, Theor. Biol. Med. Model. **2**, 4 (2005).
[4]A. W. Murray, Cell **116**, 221 (2004).
[5]D. Bell-Pedersen, S. K. Crosthwaite, P. L. Lakin-Thomas, M. Merrow, and M. Økland, Philos. Trans. R. Soc. London, Ser. B **356**, 1697 (2001).
[6]P. François, Biophys. J. **88**, 2369 (2005).
[7]A. Goldbeter, D. Gonze, G. Houart, J.-C. Leloup, J. Halloy, and G. Dupont, Chaos **11**, 247 (2001).
[8]H. H. McAdams and A. Arkin, Trends Genet. **15**, 65 (1999).
[9]H. H. McAdams and A. Arkin, Proc. Natl. Acad. Sci. U.S.A. **94**, 814 (1997).
[10]P. S. Swain, M. B. Elowitz, and E. D. Siggia, Proc. Natl. Acad. Sci. U.S.A. **99**, 12795 (2002).
[11]N. Barkai and S. Leibler, Nature (London) **403**, 267 (2000).
[12]L. Gammaitoni, P. Hanggi, P. Jung, and F. Marchesoni, Eur. Phys. J. B **69**, 1 (2009).
[13]R. Benzi, A. Sutera, and A. Vulpiani, J. Phys. A **14**, L453 (1981).
[14]D. B. Forger and C. S. Peskin, Proc. Natl. Acad. Sci. U.S.A. **102**, 321 (2005).
[15]R. Guantes and J. F. Poyatos, PLOS Comput. Biol. **2**, e30 (2006).
[16]R. Steuer, C. S. Zhou, and J. Kurths, BioSystems **72**, 241 (2003).
[17]B. Lindner, J. Garcia-Ojalvo, A. Neiman, and L. Schimansky-Geier, Phys. Rep. **392**, 321 (2004).
[18]P. Hänggi, ChemPhysChem **3**, 285 (2002).
[19]M. D. McDonnell and D. Abbott, PLOS Comput. Biol. **5**, e1000348 (2009).
[20]A. S. Pikovsky and J. Kurths, Phys. Rev. Lett. **78**, 775 (1997).
[21]M. Yi and Y. Jia, Phys. Rev. E **72**, 012902 (2005).
[22]M. Yi, Y. Jia, Q. Liu, J. R. Li, and C. L. Zhu, Phys. Rev. E **73**, 041923 (2006).
[23]G. Dupont, A. Abou-Lovergne, and L. Combettes, Biophys. J. **95**, 2193 (2008).
[24]A. Skupin, H. Kettenmann, U. Winkler, M. Wartenberg, H. Sauer, S. C. Tovey, C. W. Taylor, and M. Falcke, Biophys. J. **94**, 2404 (2008).
[25]R. Steuer, J. Theor. Biol. **228**, 293 (2004).
[26]R. Thul and M. Falcke, Phys. Rev. Lett. **93**, 188103 (2004).
[27]P. R. Patnaik, Biotechnol. Mol. Biol. Rev. **1**, 121 (2006).
[28]D. Volfson, J. Marciniak, W. J. Blake, N. Ostroff, L. S. Tsimring, and J. Hasty, Nature (London) **439**, 861 (2006).
[29]A. Ochab-Marcinek, J. Theor. Biol. **263**, 510 (2010).
[30]J. M. Raser and E. K. O'Shea, Science **309**, 2010 (2005).
[31]A. G. Fredrickson, Biotechnol. Bioeng. **18**, 1481 (1976).
[32]D. T. Gillespie, J. Phys. Chem. **81**, 2340 (1977).
[33]B. Ermentrout, *Simulating, Analyzing, and Animating Dynamical Systems: A Guide to XPPAUT for Researchers and Students* (Society for Industrial and Applied Mathematics, Philadelphia, 2002).
[34]J. D. Murray, *Mathematical Biology* (Springer-Verlag, Berlin, 1989).
[35]R. FitzHugh, J. Gen. Physiol. **43**, 867 (1960).
[36]R. FitzHugh, Biophys. J. **1**, 445 (1961).
[37]R. FitzHugh, in *Biological Engineering*, edited by H. P. Schwan (McGraw-Hill, New York, 1969).
[38]J. S. Nagumo, S. Arimoto, and S. Yoshizawa, Proc. IRE **50**, 2061 (1962).
[39]C. Rocsoreanu, A. Georgescu, and N. Giurgiteanu, *The FitzHugh-Nagumo Model: Bifurcation and Dynamics* (Kluwer, Dordrecht, 2000).
[40]E. F. Mishchenko and N. K. Rozov, *Differential Equations with Small Parameters and Relaxation Oscillations* (Plenum, New York, 1980).
[41]M. Stamatakis, Chem. Eng. Sci. **65**, 1008 (2010).
[42]S. Cooper, J. Bacteriol. **170**, 5001 (1988).
[43]D. T. Gillespie, J. Comput. Phys. **22**, 403 (1976).
[44]N. G. van Kampen, *Stochastic Processes in Physics and Chemistry* (North-Holland, New York, 1992).
[45]D. G. Manolakis, V. K. Ingle, and S. M. Kogon, *Statistical and Adaptive Signal Processing: Spectral Estimation, Signal Modeling, Adaptive Filtering and Array Processing* (McGraw-Hill, Boston, 2000).

[46]E. Schrödinger, *What is Life? The Physical Aspect of the Living Cell with Mind and Matter & Autobiographical Sketches* (Cambridge University Press, Cambridge, UK, 1992).
[47]C. W. Gardiner, *Handbook of Stochastic Methods* (Springer, Berlin, 2004).
[48]M. Stamatakis, Ph.D. thesis, Chemical and Biomolecular Engineering, Rice University, 2009.
[49]See supplementary material at E-CHAOEH-20-019003 for "Intrinsic noise and division cycle effects on an abstract biological oscillator".